Excitonic Approach for Nonadiabatic Dynamics: Extending Beyond the Frenkel Exciton Model

Eduarda Sangiogo Gil,[†] Andrea Giustini,[‡] Davide Accomasso,[¶] and Giovanni Granucci[*,‡]

†*Institute of Theoretical Chemistry, Faculty of Chemistry, University of Vienna, A-1090 Vienna, Austria*

‡*Dipartimento di Chimica e Chimica Industriale, Università di Pisa, Pisa, Italy*

¶*Faculty of Chemistry, University of Warsaw, Warsaw, Poland*

E-mail: giovanni.granucci@unipi.it

Abstract

We report the formulation and implementation of an extended Frenkel exciton model (EFEM) designed for simulating the dynamics of multichromophoric systems, taking into account of the possible presence of inter-chromophore charge transfer states, as well as other states in which two chromophores are simultaneously excited. Our approach involves constructing a Hamiltonian based on calculations performed on monomers and selected dimers within the multichromophoric aggregate. The nonadiabatic molecular dynamics is addressed using a surface hopping approach, while the electronic wavefunctions and energies required for constructing the EFEM are computed utilizing the semiempirical floating occupation molecular orbitals-configuration interaction (FOMO-CI) electronic structure method. However, our approach can in principle be adapted to ab initio methods. To validate our method, we simulate the singlet fission process in a trimer of 2,5-bis(fluorene-9-ylidene)-2,5-dihydrothiophene (ThBF) molecules, embedded in their crystal environment, comparing the results of the EFEM to the standard "supermolecule" approach.

1 Introduction

The interaction between two (or more) chromophores can lead to the migration of charge or excitation energy between them, causing changes in their electronic states.[1,2] This phenomenon is observed in various systems such as biological systems,[3–5] molecular crystals,[6–8] or covalent dimers,[9–11] where chromophores are in fixed positions and orientations. In such way, the interaction among excited states of different chromophores can persists over time, influencing the dynamics significantly.

The photoinduced nonadiabatic dynamics of an isolated chromophore can differ substantially when it interacts with surrounding chromophores.[7,12,13] Depending on the environmental conditions, various outcomes are possible: excimers may form across multiple chromophore, protons, and electrons may migrate to adjacent chromophores, and excitons can propagate through supramolecular ensembles. Understanding these interactions is crucial for the correct description of the photodynamics of multichromophoric systems.

However, conducting nonadiabatic dynamics simulations in multichromophoric systems presents significant computational challenges, necessitating the adoption of a "divide and conquer" strategy. An example of such an approach is offered by exciton models, which enable explicit full-dimensional simulations of nonadiabatic dynamics in complex multichomophoric systems.[13–17]

Recently, some of the authors have developed a Frankel exciton model that successfully describes the photodynamics of systems where local excitations (LE) dominate the dynamics.[10] However, Frenkel exciton models are designed to describe weakly coupled "monomer-like" singlet LE, i.e., multichromophoric arrays where there is no significant wavefunction overlap between the LE states. Moreover, Frenkel exciton Hamiltonians inherently lack the capability to describe charge transfer (CT) states and multiple excitations belonging to different chromophores (also designated as monomers in the following).

In recent years, several excitonic models have been proposed that extend beyond the traditional Frenkel exciton models, incorporating features like CT states, double excitations and

triplet states.[18–26] These models primarily focus on the computation of the electronic energies of the multichromophoric system. However, in order to perform on-the-fly nonadiabatic molecular dynamics simulations, there is a crucial need for the evaluation of analytical energy gradients and nonadiabatic couplings, which poses a significant challenge in this context.

Inspired by existing exciton models, particularly those outlined in Refs.,[18–20] we introduce an extension of the traditional Frenkel exciton model, hereby referred to as the *extended Frenkel exciton model* (EFEM). This model incorporates CT states and accounts for multiple excitations across two distinct chromophores, enabling for example the study of systems undergoing singlet fission (SF).

In the implementation of our Frenkel exciton model presented in Ref.,[10] a QM/MM calculation is performed for each individual monomer, where a given monomer is represented by the QM part, while the interaction with the rest of the system is taken into account at the MM level with electrostatic embedding. In the model proposed here, in addition to the QM/MM calculation performed for each individual monomer, a QM/MM calculation is performed also for each (selected) pair of chromophores, i.e. a dimer. Fig. 1 (panel A) shows a schematic representation of the different QM/MM calculations that one could perform to describe a trimer within the EFEM.

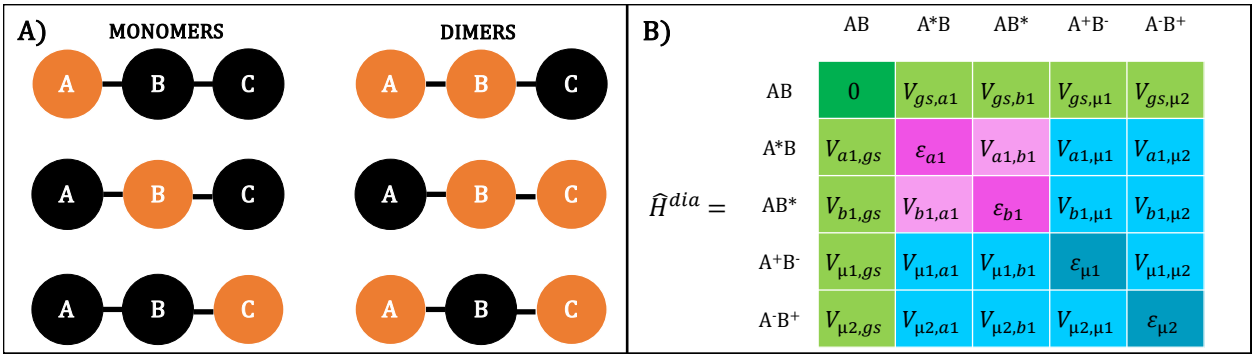

Figure 1: Panel A: Schematic representation of the QM/MM calculations to describe a trimer in the EFEM. The orange circles represents the QM part while the black ones the MM part. Panel B: Schematic representation of the diabatic Hamiltonian for a dimer AB.

We made use of the semiempirical floating occupation molecular orbitals-configuration interaction (FOMO-CI) method to evaluate the relevant electronic wavefunctions and energies.[27] However, the applicability of the approach proposed is not limited to a semiempirical framework

and can in principle be extended to ab initio approaches.

In analogy to the Frenkel exciton model proposed by us previously,[10] the exciton coupling between LE states can be computed, either exactly, within the semiempirical formalism adopted, or resorting to transition atomic charges. Instead, the couplings involving CT states are computed using a method described in Ref.,[28] where a diabatization scheme is employed in the states of the dimeric targets. This allows us to extract the diabatic state energies of each dimer and the couplings between them. The nonadiabatic molecular dynamics is here dealt with by the SH method, but the implementation we proposed is compatible with other dynamical approaches.

The paper is structured as follows: first, we describe our implementation of the EFEM in a semiempirical framework. Next, we investigate the singlet fission dynamics in a trimer of 2,5-bis(fluorene-9-ylidene)-2,5-dihydrothiophene (ThBF) molecules as a test case. In particular, the EFEM results are compared with those previously obtained by some of us[29] with the standard approach, in which the electronic structure method is applied to the whole trimer.

2 Method

In this section, we present the EFEM implementation. Hereafter, N_M represents the total number of monomers, while N_D denotes the number of dimers considered in the model. The Latin letters a, b, etc., are used to label the monomers, while the Greek letters μ, ν, etc., represent the dimers. Additionally, the Latin letters i, j, etc., are used for the states belonging to the monomers, and the Latin letters r, s, etc., are used for the states belonging to the dimers. Moreover, from now on, we will refer to the CT and multiexciton dimeric states as "non-LE".

2.1 The EFEM Hamiltonian

The EFEM electronic Hamiltonian can be expressed as follows:

$$\mathcal{H}^{EFEM} = \mathcal{H}^{FEM} + \mathcal{H}^{non-LE}. \tag{1}$$

where $\mathcal{H}^{FEM}$ is the Frenkel exciton model (FEM) Hamiltonian, which accounts for the LE states. In the present model, we maintained the same implementation of $\mathcal{H}^{FEM}$ described in a previous work by some of us,[10] which is summarized in Section 2.1.1. The $\mathcal{H}^{non-LE}$ term in Eq. 1 is added to take into account non-LE states, and includes the coupling with (some of) the LE states. Its definition is provided in Section 2.1.2.

2.1.1 LE site energies and couplings

The operator $\mathcal{H}^{FEM}$ which appears in Eq. 1 is defined as

$$\mathcal{H}^{FEM} = E_{gs}|gs\rangle\langle gs| + \sum_{a}^{N_M}\sum_{i}^{n_a}(\varepsilon_{ai} + E_{gs})|ai\rangle\langle ai| + \sum_{a,b\neq a}\sum_{i}^{n_a}\sum_{j}^{n_b} V_{ai,bj}|ai\rangle\langle bj|. \tag{2}$$

where E_{gs} is the ground-state energy (defined in Section 2.2, Eq. 9), ε_{ai} represent the so-called "site energies" of the LE states of each monomer a, $V_{ai,bj}$ is the electronic coupling between two LE states on different monomers a and b, and N_M is the total number of monomers. $|ai\rangle$ is the wavefunction of the i^{th} LE state of monomer a, which in our implementation is determined as the antisymmetrized product of the i-th excited state of monomer a with the ground states of all the other monomers, computed in separate QM/MM calculations:

$$|ai\rangle = \varphi_1^0 \wedge \varphi_2^0 \wedge \ldots \wedge \varphi_a^i \wedge \ldots \wedge \varphi_{N_M}^0. \tag{3}$$

Similarly, the ground state wavefunction $|gs\rangle$ is defined as the antisymmetrized product of the ground states of all the individual monomers:

$$|gs\rangle = \varphi_1^0 \wedge \varphi_2^0 \ldots \wedge \varphi_{N_M}^0. \tag{4}$$

To compute the coupling terms $V_{ai,bj}$, we assume that all the electronic states considered belong to the same spin manifold and that the distance between the chromophores is large enough to neglect the exchange interaction. Under these assumptions, $V_{ai,bj}$ can be approximated by the

Coulomb integral[30]

$$V_{ai,bj} \simeq \int \frac{\rho_{0i}^{(a)}(\mathbf{r}_1)\rho_{0j}^{(b)}(\mathbf{r}_2)}{r_{12}} d\mathbf{r}_1 d\mathbf{r}_2 \tag{5}$$

where $\rho_{0i}^{(a)}$ is the transition density for the two monomeric states $\varphi_0^{(a)}$ and $\varphi_i^{(a)}$, and similarly for $\rho_{0j}^{(b)}$. In the semiempirical method adopted, evaluating Eq. 5 is notably simpler compared to *ab initio* methods. This is because, within the NDO approximation, all three- and four-center two-electron integrals are neglected. Despite this simplification, determining the $V_{ai,bj}$ couplings can still be computationally demanding even for semiempirical methods. To address this issue, various approximated approaches have been developed and utilized for computing the inter-chromophore Coulomb integral. Among these, the most commum method involves simplifying transition densities to transition dipoles. This simplification enables the representation of excitonic coupling elements through the Coulomb interaction between transition dipoles. However, this approximation may lead to less reliable results when the distance between chromophores is shorter than the spatial dimension of the chromophores.[31] Here, to evaluate Eq. 5, we reduce the transition densities to a set of transition atomic charges and compute $V_{ai,bj}$ as their Coulomb interaction:

$$V_{ai,bj} \simeq \sum_{A\in a}\sum_{B\in b} \frac{q_{A,ai}q_{B,bj}}{R_{AB}} \tag{6}$$

where $q_{A,ai}$ is the transition atomic charge between the ground state and the excited state i localized at atom A on chromophore a (and similarly for $q_{B,bj}$), and R_{AB} is the distance between atoms A and B. The transition atomic charges are obtained using the TrESP method,[32] which involves the fitting of the electrostatic potential arising from a given electron density. We stress that in our previous study, when we calculated excitonic couplings using Eq. 6, the outcomes of nonadiabatic dynamics were practically indistinguishable from those obtained when evaluating excitonic couplings with Eq. 5.[10] Therefore, we regard this approximation as suitable for computing the coupling between LE.

In order to construct $\mathcal{H}^{FEM}$ (Eq. 2), a series of N_M QM/MM calculations is performed, in each of which a given chromophore a represents the QM moiety, while the rest of the system is

treated at the MM level with electrostatic embedding. From the QM/MM calculations we have then access to the individual chromophores energies ε_{ai} and wavefunctions φ_a^i, from which $|ai\rangle$ and $V_{ai,bj}$ (Eq. 3 and 6) are computed.

2.1.2 Non-LE site energies and couplings

The non-LE part of the EFEM Hamiltonian (Eq. 1) is defined as follows:

$$\begin{aligned}\mathcal{H}^{non-LE} = &\sum_{\mu}^{N_D}\sum_{r}^{n_\mu}(\varepsilon_{\mu r} + E_{gs}^{\mu})|\mu r\rangle\langle\mu r| + \sum_{\mu}^{N_D}\sum_{r}^{n_\mu}\sum_{a\in\mu}^{N_M}\sum_{i}^{n_a} V_{\mu r,ai}|\mu r\rangle\langle ai| + \\ &+ \sum_{\mu}^{N_D}\sum_{r}^{n_\mu}\sum_{s\neq r}^{n_\mu} V_{\mu r,\mu s}|\mu r\rangle\langle\mu s|\end{aligned} \tag{7}$$

where $\varepsilon_{\mu r}$ represent the site energies for the non-LE states, E_{gs}^{μ} is a dimer-specific ground state energy (defined in Section 2.2, Eq. 10), $V_{\mu r,ai}$ is the electronic coupling between a LE state and a non-LE state, $V_{\mu r,\mu s}$ represents the coupling between two non-LE states, and N_D is the total number of considered dimers. Moreover, $|\mu r\rangle$ represents the r^{th} electronic excited state localized on dimer μ and n_μ is the number of states $|\mu r\rangle$ considered. In our approach, we determine $|\mu r\rangle$ as the antisymmetrized product of the r-th diabatic state of a specific dimer μ with the ground states of all other monomers which do not belong to the considered dimer (μ):

$$|\mu r\rangle = \varphi_1^0 \wedge \varphi_2^0 \wedge \ldots \wedge \varphi_\mu^r \wedge \ldots \wedge \varphi_{N_M}^0. \tag{8}$$

It is important to note that in Eq. 7 only the electronic couplings between LE states and non-LE states within the same dimer are taken into account. This is reflected in the third term on the right-hand side of Eq. 7, where a must belong to μ. Additionally, the electronic couplings between non-LE states of different dimers, denoted as $V_{\mu r,\nu s}$ with $\mu \neq \nu$, are neglected (i.e. set to zero) in Eq. 7. However, we note that the absence of these electronic couplings does not exclude the possibility of having transitions between non-LE of different dimers during the dynamics, as these states can interact through the nonadiabatic couplings (evaluated as described in Section

2.5).

The site energies $\varepsilon_{\mu r}$, couplings $V_{\mu r,ai}$ and $V_{\mu r,\mu s}$, and wavefunctions φ^r_μ are obtained performing separated QM/MM calculations for each of the N_D dimers. However, the procedure is more complex than for the monomers, as it involves a diabatization step. In particular, from a QM/MM calculation for a dimer, the electronic adiabatic states of the given dimer are computed. Next, to define the LE and non-LE states, we use a diabatization scheme previously developed by some of us.[28] Specifically, for each QM dimer, we first localize the molecular orbitals (MOs) on the two monomers, and then diabatic states are determined by rotating the (previously computed) adiabatic states so as to maximize the overlap with a predefined set of references,[28] which are models for the LE and non-LE states of interest. The same rotation matrix is used to build a diabatic Hamiltonian for each dimer, from which the site energies $\varepsilon_{\mu r}$ and couplings $V_{\mu r,ai}$ and $V_{\mu r,\mu s}$ are extracted. On the other hand, the site energies of LE states and couplings between them, obtained from the diabatization, are discarded, as these quantities are computed from monomeric QM/MM calculations, as described in Section 2.1.1. A consequence is that the states $|\mu r\rangle$ and $|ai\rangle$ with $a \in \mu$, which are assumed to be orthogonal, are only approximately so, as they are built with different sets of molecular orbitals. In the present implementation this poses no problem, as the coupling between these states is evaluated as the electronic coupling $V_{\mu r,ai}$ (through the diabatization procedure referred above), rather than as nonadiabatic coupling.

As a typical example, let's consider a dimer consisting of monomers a and b, for which the following diabatic states are computed: the ground state (AB), two LE states localized on either monomer a (A^*B) or b (AB^*), and two charge transfer states (A^+B^- and A^-B^+). The Hamiltonian in this diabatic basis is shown in Figure 1B. The first diagonal matrix element is the energy of the ground state AB of the dimer, which is set to zero for simplicity. The light green elements are the couplings between AB and the excited states. The dark pink elements are the site energies of the two LE states A^*B and AB^*, while the light pink elements represent the electronic couplings between them. Finally, the dark blue elements correspond to the site energies of the non-LE states A^+B^- and A^-B^+, and the light blue elements represent the electronic couplings

between the non-LE states and between a non-LE state and a LE state. From a QM/MM calculation on the dimer, we only extract the dark and light blue elements of the Hamiltonian in Figure 1B, while the pink and green elements are not utilized.

2.2 Ground-state energy

The EFEM ground-state energy is defined as

$$E_{gs} = \sum_{a}^{N_M} [E(QM/MM, a)] - (N_M - 1)E(MM) \tag{9}$$

where $E(MM)$ represents the energy of the whole system calculated at the MM level, and $E(QM/MM, a)$ is the ground-state QM/MM energy of monomer a. A detailed derivation of Eq. 9 is provided in Sec. S1 of the SI.

E_{gs} is used to compute the energy of each LE state, defined as the sum of E_{gs} and the corresponding site energy (Eq. 2). Instead, for the energies of the non-LE states, we had to introduce dimer-specific ground-state energies E^{μ}_{gs}, defined as follows:

$$\begin{aligned} E^{\mu}_{gs,0} &= \sum_{a \notin \mu}^{N_M} [E(QM/MM, a)] + E(QM/MM, \mu) - (N_M - 2)E(MM) \\ E^{\mu}_{gs} &= E^{\mu}_{gs,0} + \lambda(\mu). \end{aligned} \tag{10}$$

In Eq. 10, $E(QM/MM, a)$ is the ground-state QM/MM energy of monomer a (not belonging to dimer μ), $E(QM/MM, \mu)$ is the diabatic ground-state QM/MM energy of dimer μ, and $\lambda(\mu)$ is an empirical shift dependent on the specific dimer considered, which was introduced to ensure consistency between the absolute energies of non-LE states and those of LE states. In principle, $\lambda(\mu)$ could depend on the nuclear coordinates, but in practice that dependence is needed only if the monomers are subject to large rearrangements. In particular, in the test case we have considered (see section 3, equation 17), it was possible to take $\lambda(\mu)$ as a constant.

2.3 Adiabatic states

The diagonalization of the EFEM electronic Hamiltonian $\mathcal{H}^{EFEM}$ (Eq. 1) yields the electronic adiabatic wavefunctions (the ground-state $|gs\rangle$ and the excited states $|K\rangle$), and the corresponding energies E_{gs} (Eq. 9) and E_K. The wavefunctions $|K\rangle$ are linear combinations of $|ai\rangle$ and $|\mu r\rangle$ (defined in Eqs. 3 and 8):

$$|K\rangle = \sum_{a,i} c_{ai,K}|ai\rangle + \sum_{\mu,r} c_{\mu r,K}|\mu r\rangle \tag{11}$$

where $c_{ai,K}$ and $c_{\mu r,K}$ are the elements of the orthogonal matrix $\boldsymbol{c}$ that diagonalizes $\mathcal{H}^{EFEM}$. Therefore, the corresponding adiabatic energies E_K are given by

$$\begin{aligned} E_K = &\sum_{a,i} |c_{ai,K}|^2(\varepsilon_{ai} + E_{gs}) + \sum_{c,i}\sum_{b,j} c_{ai,K}c_{bj,K}V_{ai,bj} + \\ &+ \sum_{\mu,r} |c_{\mu r,K}|^2(\varepsilon_{\mu r} + E^{\mu}_{gs}) + \sum_{\mu,r}\sum_{a,i} c_{\mu r,K}c_{ai,K}V_{\mu r,ai} + \sum_{\mu,r}\sum_{\mu,s} c_{\mu r,K}c_{\mu s,K}V_{\mu r,\mu s}. \end{aligned} \tag{12}$$

We anticipate that, in our EFEM implementation, the adiabatic basis so obtained is employed for the time propagation of the SH trajectories, as SH works best in the adiabatic representation.[33] In fact, unlike the electronic couplings (here represented by the off-diagonal elements of $\mathcal{H}^{EFEM}$), the nonadiabatic couplings are well localized in regions of near degeneracy, thereby minimizing the number of transitions required and reducing the need for extensive velocity rescaling after a hop. This is especially important in multichromophoric systems, to avoid nonphysical transitions between distant monomers. Additionally, working in the adiabatic representation eliminates the need for special considerations regarding the superexchange effect.[29,34]

2.4 Energy gradients

The gradients of the ground state energy E_{gs} and of the dimer specific energies E^{μ}_{gs} (Eq. 9 and 10) with respect to nuclear coordinates are computed using the gradients of the QM/MM ground state energies of all monomers a and dimers μ, and the gradient of the MM energy for the whole

system.

The calculation of the energy gradients of the adiabatic excited states K requires computing the derivatives of the $\mathcal{H}^{EFEM}$ matrix elements with respect to nuclear coordinates, while the derivatives of the variationally optimized coefficients $c_{ai,K}$ and $c_{\mu r,K}$ (obtained by diagonalizing $\mathcal{H}^{EFEM}$) do not contribute to the gradients. Specifically, the gradient of a given adiabatic excited state K is given by

$$\begin{aligned}\nabla E_K = &\sum_{a,i} |c_{ai,K}|^2 (\nabla \varepsilon_{ai} + \nabla E_{gs}) + \sum_{c,i} \sum_{b,j} c_{ai,K} c_{bj,K} \nabla V_{ai,bj} + \\ &+ \sum_{\mu,r} |c_{\mu r,K}|^2 (\nabla \varepsilon_{\mu r} + \nabla E^{\mu}_{gs}) + \sum_{\mu,r} \sum_{a,i} c_{\mu r,K} c_{ai,K} \nabla V_{\mu r,ai} + \\ &+ \sum_{\mu,r} \sum_{\mu,s} c_{\mu r,K} c_{\mu s,K} \nabla V_{\mu r,\mu s}.\end{aligned} \tag{13}$$

The derivatives of the LE site energies, $\nabla \varepsilon_{ai}$, are obtained from the monomeric QM/MM calculations as the difference between the gradient of the energy of the excited state φ^i_a and the gradient of the energy of the ground state φ^0_a of monomer a. The gradients of the couplings between LE, $\nabla V_{ai,bj}$, are obtained as derivatives of Eq. 6 with the assumption of neglecting the dependence of the transition charges $q_{A,ai}$ on the nuclear coordinates.[10]

The calculation of the derivatives of the non-LE site energies $\nabla \varepsilon_{\mu r}$, as well as of the electronic couplings $\nabla V_{\mu r,ai}$ and $\nabla V_{\mu r,\mu s}$, requires computing the gradients of the diabatic Hamiltonian for each dimer μ. Assuming that the diabatic states of each dimer do not depend on the nuclear coordinates (i.e. that they are strictly diabatic states), the derivative of the diabatic Hamiltonian $\boldsymbol{H}^{dia}$ with respect to a nuclear coordinate, Q_α, is given by

$$\frac{\partial \boldsymbol{H}^{dia}}{\partial Q_\alpha} = \boldsymbol{T}^\dagger \frac{\partial \boldsymbol{E}}{\partial Q_\alpha} \boldsymbol{T} + \boldsymbol{T}^\dagger \boldsymbol{G}_\alpha \boldsymbol{T} \tag{14}$$

$$\boldsymbol{G}_\alpha = \boldsymbol{g}_\alpha \boldsymbol{E} - \boldsymbol{E} \boldsymbol{g}_\alpha \tag{15}$$

where $\boldsymbol{E}$ is a diagonal matrix containing the energies of the adiabatic states of the dimer, $\boldsymbol{g}_\alpha$

is the nonadiabatic coupling matrix, and $\boldsymbol{T}$ is the unitary matrix that transforms the adiabatic basis into the diabatic one. A detailed derivation of Eq. 14 is provided in Section S2 of the SI. Once $\frac{\partial \boldsymbol{H}^{dia}}{\partial Q_\alpha}$ has been computed (using Eq. 14), the derivatives $\nabla V_{\mu r,ai}$ and $\nabla V_{\mu r,\mu s}$ are extracted from the off-diagonal elements of $\frac{\partial \boldsymbol{H}^{dia}}{\partial Q_\alpha}$, while its diagonal elements are used to compute $\nabla \varepsilon_{\mu r}$, determined as the difference between the gradient of the energy of the excited state φ^r_μ and the gradient of the energy of the ground state φ^0_μ of dimer μ.

2.5 Nonadiabatic dynamics

In our EFEM implementation, the nonadiabatic dynamics of the multichromophoric system is treated using Tully's fewest switches surface hopping (FSSH).[35] In particular, the nuclear wavepacket dynamics is approximated using a swarm of independent classical trajectories, each propagated on the adiabatic states obtained by diagonalization of $\mathcal{H}^{EFEM}$ (Section 2.3). Along each trajectory, the electronic time-dependent Schrodinger equation (TDSE) is integrated and the electronic coefficients are used to compute transition probabilities between states, which are employed at each time step to decide whether a nonadiabatic transition (i.e. a hop) can occur.

In this work, we adopt the local diabatization (LD) formulation of FSSH.[36] At variance with the standard implementation of FSSH, the LD algorithm is exempt from problems caused by crossings between (almost) noninteracting electronic states (often termed "trivial unavoided crossings"), which are common in multichromophoric systems, making LD particularly well-suited for investigating the dynamics of such systems. In the LD scheme, the nonadiabatic coupling vectors are not explicitly computed, but the wavefunction overlap matrix within a given time step is required to integrate the electronic TDSE. In general, the wavefunction overlap matrix element between two adiabatic states K and L for a given time step $\Delta t'$ of the nuclear trajectory is defined as

$$S_{KL}(t, t + \Delta t') = \langle K(t) | L(t + \Delta t') \rangle \,. \tag{16}$$

Within the semiempirical framework adopted in this work, the molecular orbitals (MOs) ob-

tained from QM/MM calculations for different monomers or dimers are orthogonal, because they are linear combinations of distinct sets of orthogonal atomic orbitals (AOs). In this context, the calculation of the wavefunction overlap matrix (Eq. 16) simplifies significantly, as described in detail in Section S3 of the SI. In a nutshell, the wavefunction overlap between LE states is given by the product of the overlaps of the individual monomers, while the overlap between non-LE states of the same dimer requires the additional evaluation of the wavefunction overlap $\left\langle \varphi^r_{(ab)}(t) | \varphi^s_{(ab)}(t+\Delta t') \right\rangle$. For the latter, we assume that the dimer states are strictly diabatic and we set that integral to one if $s = r$, and to zero if $s \neq r$. The same hypothesis is employed for the overlaps between LE and non-LE with a monomer in common, which in our implementation are set to zero. On the other hand, the calculation of the overlap between non-LE states of dimers sharing one monomer (e.g. ab and bc) is more complicated and requires the construction of "trimer-like" wavefunctions, each combining a monomer and a dimer wavefunction, which are then used to evaluate the integrals $\left\langle \varphi^r_{(ab)}(t) \wedge \varphi^0_c(t) | \varphi^0_a(t+\Delta t') \wedge \varphi^s_{(bc)}(t+\Delta t') \right\rangle$. Additionally, all the overlaps between non-LE states of two distinct dimers (i.e. without a monomer in common) are equal to zero, due to the orthogonality of their MOs.

We note that the cost of computing overlaps between trimer-like wavefunctions can increase significantly, because of the large number of Slater determinants involved. One strategy to alleviate this issue is to consider only determinants with CI coefficients above a certain threshold, followed by wavefunction renormalization. The calculation of those trimer-like overlaps is important in our EFEM implementation because it allows for transitions between non-LE states of dimers with only one monomer in common, for which the electronic couplings are neglected (Section 2.1.2).

2.6 EFEM dynamics workflow

In our EFEM implementation, the semiempirical QM/MM calculations for monomers and dimers are done with MOPAC-PI,[37] interfaced with the molecular mechanics TINKER 8.5 program package.[38] The SH dynamics is performed using the Newton-X package,[39] modified to run the exciton

dynamics. The workflow of the EFEM SH dynamics is as follows:

1. Perform monomeric QM/MM calculations (one for each monomer);
2. Perform dimeric QM/MM calculations, including diabatization;
3. Perform an MM calculation for the entire system;
4. Using the results from steps 1-3, construct and diagonalize $\mathcal{H}^{EFEM}$, compute the adiabatic energy gradients (Section 2.4) and the overlap matrix (Eq. 16, Section 2.5);
5. Provide energies, gradients, and the wavefunction overlap matrix to the driver responsible for nuclear dynamics, which integrates the electronic TDSE, assesses hopping probabilities, and calculates the new nuclear coordinates and velocities;
6. Repeat steps 1-5 until the desired trajectory endpoint.

To reduce the total computation time, the calculations of steps 1-3 can be executed in parallel.

3 Test case: singlet fission dynamics in ThBF

As a test case for our EFEM implementation, we investigate the singlet fission (SF) process in a trimer of ThBF embedded in its crystal environment (Fig. 2). The same system was studied by some of us using a standard QM/MM scheme in which the whole trimer was the QM part, while the rest of the crystal was described at the MM level.[29] The latter work, referred to as "trimer-full-QM" from now on, will be used here as a reference to assess our proposed EFEM. We believe that the selected system is a good test case for EFEM, because its SF dynamics involves not only LE states but also two different kinds of non-LE, namely the multiexciton double triplet states (TT) and the CT states.

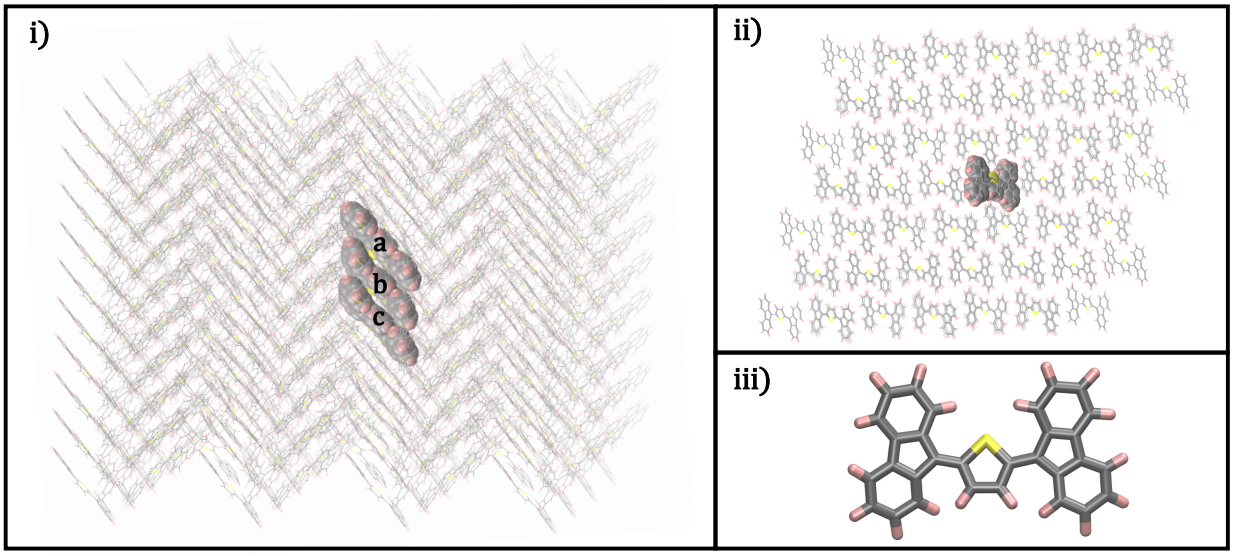

Figure 2: i) Side view of the ThBF crystal, ii) top view of the ThBF crystal and iii) ThBF monomer. The S atoms are in yellow, the C atoms are in gray and the H atoms are in pink. The highlighted trimer was investigated using EFEM.

3.1 Computational details

The dynamics simulations were performed using the same crystalline cluster of ThBF considered for the trimer-full-QM calculations in our previous work.[29] In particular, we have considered a cluster containing 490 ThBF molecules, arranged in a 7x7 array of columns, each containing 10 slip-stacked molecules. The three molecules highlighted in Fig. 2, which are in the center of the cluster, were treated using EFEM. All the other molecules of the cluster were described at the MM level. To preserve the crystal structure during the dynamics, the coordinates of 162 MM molecules at the boundary of the cluster were frozen during the dynamics, while the other 328 molecules were free to move.

The electronic energies and wavefunctions of the QM monomers and dimers were obtained using the FOMO-CI method[36] with the semiempirical PM3 Hamiltonian,[40] previously re-parametrized for the ThBF molecule.[41] Each ThBF monomer was treated with an active space of 2 MOs and 2 electrons. Consistently, for each dimer, an active space of 4 MOs and 4 electrons was used. In the QM/MM calculations, the MM molecules were described using the OPLS force field and

the interaction between the QM and MM subsystems was treated with electrostatic embedding.[42] We note that, at each time step of our EFEM simulations, six QM/MM calculations are required: three monomeric QM/MM calculations and three additional QM/MM calculations for the following dimers: ab, bc, and ac. In particular, the QM/MM calculations for the dimers included the diabatization procedure referred above (see section 2.1.2), from which 6 diabatic states are obtained, representing (considering dimer ab) the ground state AB, the two localized excitations on the two monomers (A^*B and AB^*), the TT state, and two CT states (A^+B^- and A^-B^+). The diabatization was performed by rotating the first 12 adiabatic singlet states in order to maximise the overlap with respect to the 6 reference models representing the diabatic states wanted. This choice (using a larger number of adiabatic states with respect to the diabatic references) allowed to avoid problems with intruder states. To reduce the computational cost, the gradient of each dimeric diabatic Hamiltonian was computed by neglecting the second term in the RHS of Eq. 14, according to the hypothesis that $\boldsymbol{G}_\alpha \approx 0$. This approximation was tested and validated as described in Section S4 of the SI.

A distribution of coordinates and velocities was generated by performing a ground-state thermal equilibration of the QM/MM system at 300 K with the Andersen thermostat,[43] which was propagated for 14 ps. A total of 98 initial conditions (i.e., coordinates and velocities) were extracted from the last 10 ps of the thermalization and the corresponding initial electronic states were selected according to their transition dipoles from the ground state within an energy window ranging from 2.25 eV to 2.45 eV. In the SH simulations, we used the LD algorithm for the integration of the electronic TDSH,[36] with an integration time step of 0.1 fs (both for the nuclear and the electronic degrees of freedom). The overlap quantum decoherence correction scheme[44,45] was applied to each trajectory with the Gaussian width $\sigma = 1.0$ a.u. and the minimum overlap threshold $S_{min} = 0.005$ to be consistent with Ref.[29] The rescaling of the nuclear velocities after a hop was performed in the direction of the nuclear momentum.

The $\lambda(\mu)$ constant shifts for the dimer ground-state energies (Eq. 10) were defined at the

starting geometry of each trajectory according to the following equation

$$\lambda(\mu) = E_{gs}(t=0) - E^{\mu}_{gs,0}(t=0) + \Delta \tag{17}$$

where E_{gs} end $E^{\mu}_{gs,0}$ are defined in Eqs. 9 and 10, respectively. The constant $\Delta = 0.5$ eV was introduced in order to obtain starting energies that are in agreement with the trimer-full-QM ones.[29]

We have considered a basis of 13 diabatic states, as schematically represented in Fig. 3. In particular, these states are the ground state $S_0S_0S_0$, three LE states ($S_1S_0S_0$, $S_0S_1S_0$, and $S_0S_0S_1$), and 9 non-LE states. The latter are represented by three singlet combination of two triplets, TTS_0, TS_0T and S_0TT; and six CT states $A^+B^-S_0$, $A^-B^+S_0$, $A^+S_0C^-$, $A^-S_0C^+$, $S_0B^+C^-$ and $S_0B^-C^+$, where A, B and C indicate the three monomers treated with EFEM.

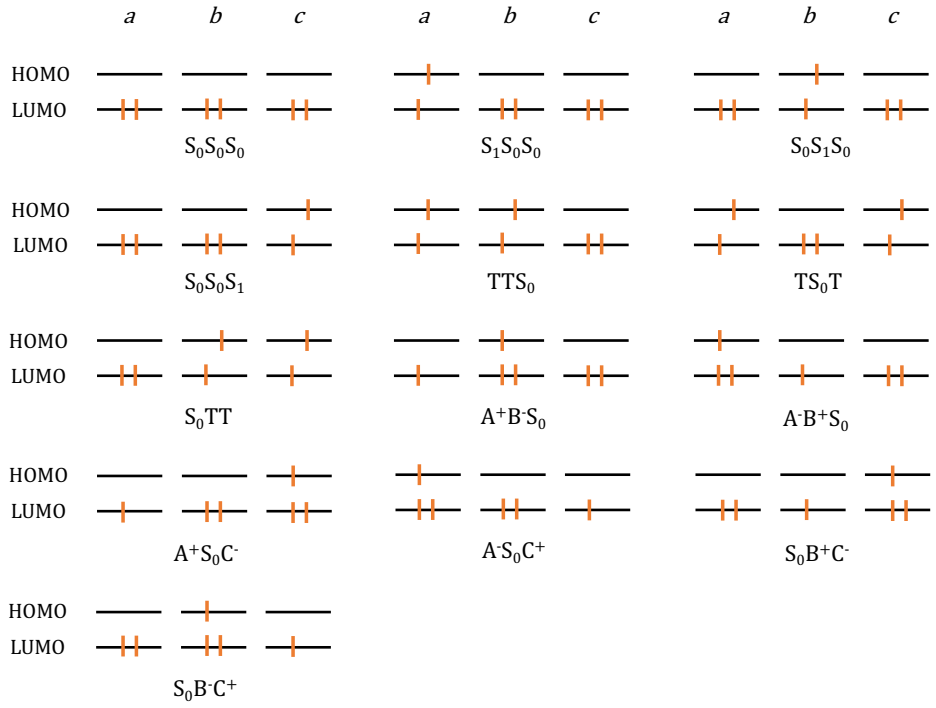

Figure 3: Schematic representation of the diabatic states included in the EFEM simulations for the ThBF trimer.

As in our previous work,[29,46] we found it convenient to analyse the SF dynamics simulations

using an alternative basis of electronic states, hereafter referred to as the excitonic basis. The latter was defined by diagonalizing two specific blocks of the electronic Hamiltonian matrix in the diabatic basis, corresponding to the 3×3 submatrix of the LE states, and the 6×6 block of the CT states. In this way, the following excitonic states are obtained: (i) three delocalized combinations of LE, labelled $S^{\star}_{1-3}$, (ii) the three TT states (TTS_0, S_0TT, and TS_0T), and (iii) six delocalized CT states, CT_{1-6}.

3.2 Ground state thermal dynamics and absorption spectrum

In Fig.4 we present the transition energies in the excitonic representation, obtained from the ground state thermal equilibration. These energies closely match the ones obtained in the trimer-full-QM simulations,[29] the main difference being a slightly larger spacing among the CT states. From Fig. 4, it can be observed that the excitation energies of the three TT states (TTS_0, S_0TT, and TS_0T) oscillate around $\sim$1.7 eV, in good agreement with the trimer-full-QM. The standard deviation of the TT energies is about 0.19 eV in our EFEM simulations, which is very close to the value of 0.2 eV for the trimer-full-QM. The LE state energies oscillate around 2.1 eV in both the EFEM and the trimer-full-QM simulations, with much smaller fluctuations compared to the TT states, the standard deviation of LE being 0.04 eV and 0.03 eV for EFEM and trimer-full-QM, respectively. This difference in energy fluctuations between LE and TT can be attributed to the more steep potential energy surface of the TT states in the Franck-Condon region compared to LE states, as indicated by the difference between vertical and adiabatic transition energies: 0.37 eV for the TT and 0.01 eV for LE states.[41]

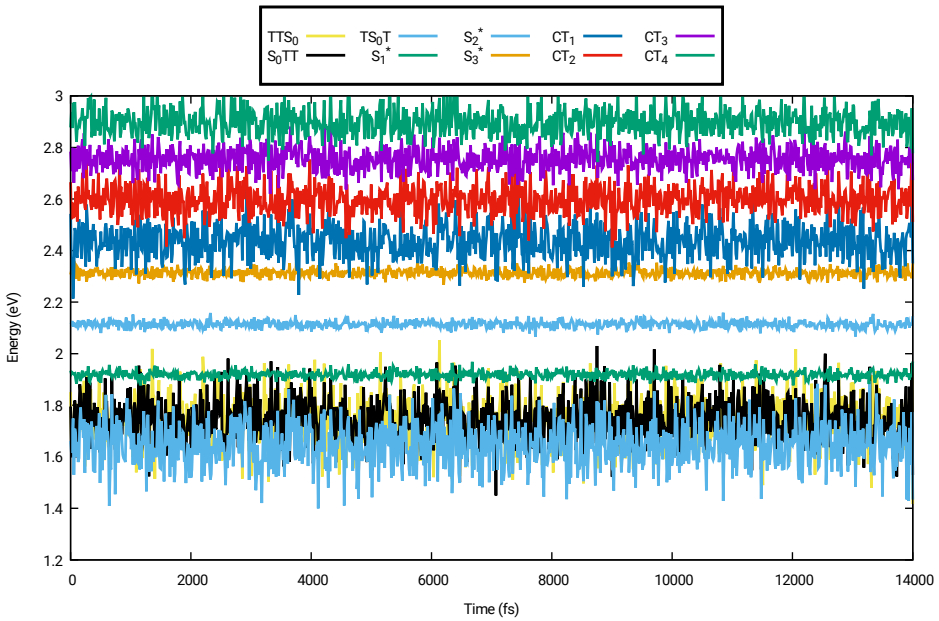

Figure 4: Transition energies (eV) in the excitonic representation, obtained from the ground state thermal equilibration of the ThBF trimer embedded in its crystalline environment. The reported results are obtained by averaging over time intervals of 20 fs.

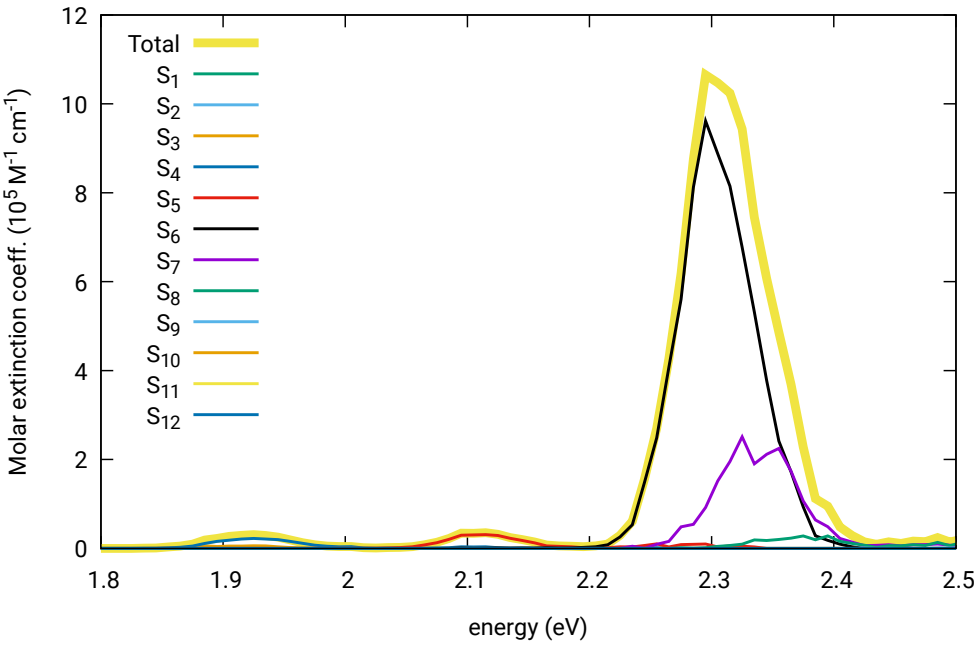

Figure 5: Absorption spectrum obtained from the ground state thermal equilibration of the ThBF trimer using EFEM.

The transition energies evaluated along the thermalization trajectory, together with the tran-

sition dipoles, were used to calculate the absorption spectrum reported in Fig. 5. If compared to the trimer-full-QM results,[29] the absorption spectrum calculated with the EFEM model show a very good agreement, apart from a red-shift of approximately 0.3 eV. Despite this shift, the maximum of the most intense band agrees well with the spectroscopic data: 2.30 eV in toluene solution and approximately 2.38 eV in crystalline thin film.[47]

To characterize the nature of the electronic states, in Table 1 we report the squared overlaps of the adiabatic states with the excitonic basis, averaged along the thermal equilibration. Notably, the S_6 state is most of the time the brightest combination of LE and provides the most important contribution to the spectrum, in agreement with the trimer-full-QM results.[29] During the ground-state dynamics, the S_6 state can acquire a significant contribution from the CT_1 state and, at those geometries, the bright state becomes S_7 or even S_8. The latter states are most of the time of CT character, while the lower-lying S_4 and S_5 states are most often dark combinations of LE and contribute to the absorption spectrum with weak bands centered at approximately 1.95 eV and 2.12 eV, respectively. The three low-lying excited states S_1, S_2, and S_3 are dominated by the double triplet states TTS_0, S_0TT, and TS_0T. Since the transition from $S_0S_0S_0$ to the TT states is optically forbidden, those states do not contribute significantly to the absorption spectrum.

Table 1: Average weights (squared overlaps) of the excitonic states in the 12 lower lying singlet adiabatic states obtained from the ground state thermal equilibration. Only weights ≥ 0.1 are reported in parentheses. The averaged transition energies (in eV) are also shown, together with the squared transition dipole moments (in au).

State	Energy (eV)	excitonic states (weights)	$\mu^2_{S_0 \to S_n}$ (au)
S_0	0.000	$S_0S_0S_0$ (1.00)	–
S_1	1.578	TTS_0 (0.24), S_0TT (0.21), TS_0T (0.52)	0.03
S_2	1.710	TTS_0 (0.28), S_0TT (0.35), TS_0T (0.27)	0.15
S_3	1.808	S_1^* (0.21), TTS_0 (0.32), S_0TT (0.30), TS_0T (0.16)	0.35
S_4	1.952	S_1^* (0.67), TTS_0 (0.13), S_0TT (0.11)	1.53
S_5	2.117	S_2^* (0.92)	2.08
S_6	2.293	S_3^* (0.76), CT_1 (0.21)	43.80
S_7	2.454	S_3^* (0.20), CT_1 (0.77)	12.54
S_8	2.599	CT_2 (0.97)	3.48
S_9	2.755	CT_3 (0.99)	0.45
S_{10}	2.898	CT_4 (1.00)	0.08
S_{11}	3.545	CT_5 (1.00)	0.00
S_{12}	3.865	CT_6 (1.00)	0.00

The largest electronic couplings are found between first neighbor LE states. In particular, $\langle S_1S_0S_0|\hat{H}_{el}|S_0S_1S_0\rangle$ and $\langle S_0S_0S_1|\hat{H}_{el}|S_0S_1S_0\rangle$, averaged over the thermalization trajectory, evaluate respectively to 138 and 131 meV, in very good agreement with the trimer-full-QM result[29] (131 and 134 meV). This agreement is not surprising, considering that the exchange interaction is neglected in the semiempirical framework.[10] However, it is a confirmation that the Coulomb coupling between LE states is correctly represented by the interaction between transition charges. In Table 2 we report the electronic Hamiltonian matrix elements in the excitonic basis, computed with EFEM and averaged over the thermalization trajectory. In comparing with the trimer-full-QM results, one has to take into account that in EFEM the couplings with the ground state $S_0S_0S_0$ are zero by construction. For all the other couplings, the agreement with the trimer-full-QM re-

sults[29] can be considered as semiquantitative, with vanishingly small $\hat{H}_{el}$ matrix elements (of the order of 0.1 meV or less) between S^* and TT states, and larger couplings between S^* and CT states and between TT and CT states. In particular, we stress that both the couplings between non-LE states and the couplings between LE and non-LE states are well reproduced.

Table 2: Average electronic Hamiltonian matrix in the excitonic representation, obtained from the ground state thermal equilibration of the ThBF trimer using EFEM. All the matrix element are expressed in meV. For the off diagonal matrix elements, the absolute value is considered, and only the elements ≥ 0.1 meV are shown. The matrix elements involving CT_5 and CT_6 are not reported.

$\hat{H}_{el}$	$S_0S_0S_0$	TTS_0	S_0TT	TS_0T	S_1^*	S_2^*	S_3^*	CT_1	CT_2	CT_3	CT_4
$S_0S_0S_0$	0.0	0	0	0	0	0	0	0	0	0	0
TTS_0	0	1748	0.0	0.0	0.1	0.1	0.1	2.8	3.1	6.2	8.0
S_0TT	0	0.0	1743	0.0	0.1	0.1	0.1	3.2	5.7	9.7	9.6
TS_0T	0	0.0	0.0	1654	0.0	0.0	0.0	0.0	0.0	0.0	0.0
S_1^*	0	0.1	0.1	0.0	1918	0	0	9.1	9.4	7.2	6.3
S_2^*	0	0.1	0.1	0.0	0	2114	0	7.3	7.4	6.2	6.2
S_3^*	0	0.1	0.1	0.0	0	0	2313	9.4	9.0	7.5	6.3
CT_1	0	2.8	3.2	0.0	9.1	7.3	9.4	2434	0	0	0
CT_2	0	3.1	5.7	0.0	9.4	7.4	9.0	0	2597	0	0
CT_3	0	6.2	9.7	0.0	7.2	6.2	7.5	0	0	2754	0
CT_4	0	8.0	9.6	0.0	6.3	6.2	6.3	0	0	0	2897

3.3 Simulation of the excited state dynamics

In this section, we present the surface hopping (SH) nonadiabatic dynamics simulations for the ThBF trimer that we performed using EFEM. A total of 98 SH trajectories were computed. 71 trajectories were initiated from S_6, 22 from S_7, 4 from S_8, and 1 from S_5.

Figure 6a shows the time evolution of the excitonic state populations, averaged over all the SH trajectories, that we obtained in the EFEM simulations. The corresponding adiabatic and diabatic populations are reported in Figures S6 and S7 of the SI. For comparison, in Figure 6b we also report the excitonic state populations obtained in the trimer-full-QM simulations.[29] To facilitate the analysis of the simulations, in Figure 6 the CT states, the dark excitonic states S_2^* and S_1^*, and the TT states are grouped together. Moreover, in Table 3 we report the total number of hops

between of excitonic states obtained in the SH simulations using EFEM.

At the beginning of the simulation, the most populated state is S_3^*, which is the bright combination of the LE states. However, a non negligible fraction (20%) of the starting population is found on CT states (mainly CT_1 and CT_2). In the first 500 fs after the excitation, S_3^* decays to the dark combinations of LE, S_2^* and S_1^*, and to a lesser extent to the CT states (Figure 6a and Table 3). Additionally, the CT states acquire population from the LE states, as indicated by the negative net flow for the CT $\rightarrow S_{1-2}^*$ and for the CT $\rightarrow S_3^*$ transitions in Table 3 (0-500 fs). At longer times ($>$ 500 fs), both the dark excitonic states, S_2^* and S_1^*, and the CT states transfer most of their population to the TT states (Table 3, 500-4000 fs), which are the most populated states at the final time of the simulations (4000 fs, Figure 6a). These fluxes of population are schematically illustrated in Figure 7.

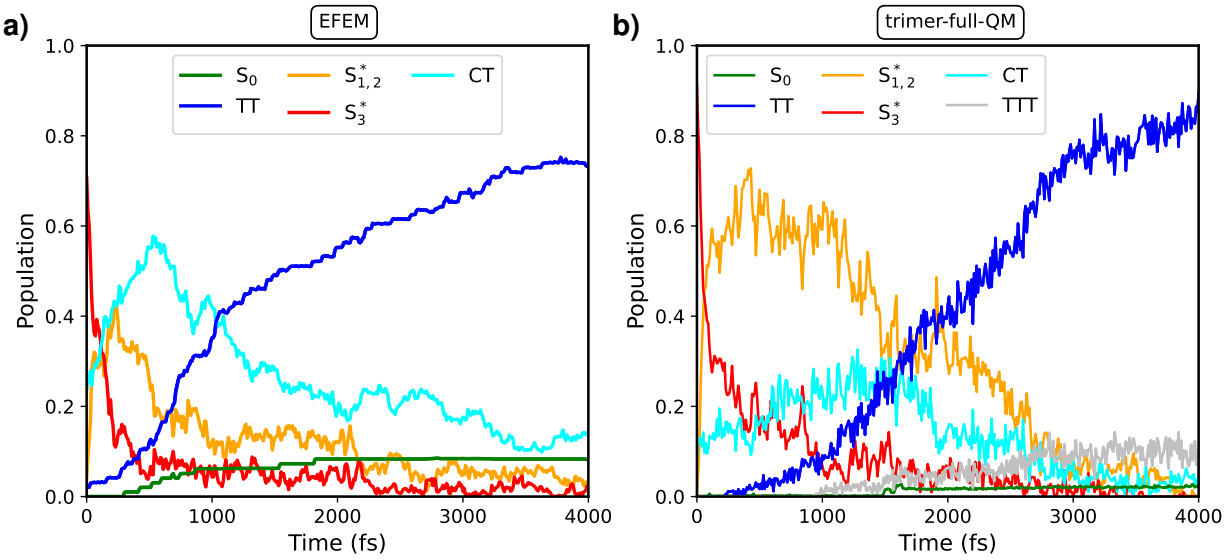

Figure 6: Populations of the excitonic states as functions of time, obtained in the surface hopping simulations using EFEM (this work, panel a) and in the simulations based on the trimer-full-QM (populations taken from Ref.,[29] panel b). The double triplet, the dark excitonic, and the charge transfer states are grouped together and indicated as TT, $S_{1,2}^*$, and CT, respectively. The reported populations are obtained by averaging over all the surface hopping trajectories and time intervals of 10 fs.

Table 3: Transitions between pairs of excitonic states (i, j). The charge transfer, the dark excitonic and the double triplet states are grouped together and indicated as CT, $S^*_{1,2}$, and TT, respectively. Presented are the number of transitions for two distinct time ranges (0-500 fs and 500-4000 fs). The net flow is the difference between the $i \rightarrow j$ and the $j \rightarrow i$ transitions. We recall here that the total number of trajectories is 98.

States		0-500 fs			500-4000 fs		
i	j	$i \rightarrow j$	$j \rightarrow i$	net	$i \rightarrow j$	$j \rightarrow i$	net
S^*_{1-2}	S_0	2	0	2	6	1	5
S^*_3	S_0	0	0	0	1	0	1
S^*_{1-2}	TT	5	4	1	37	19	18
S^*_3	TT	1	1	0	11	8	3
CT	TT	10	2	8	72	32	40
S^*_3	S^*_{1-2}	143	86	57	288	278	10
CT	S^*_{1-2}	98	129	-31	459	468	-9
CT	S^*_3	104	119	-15	272	262	10

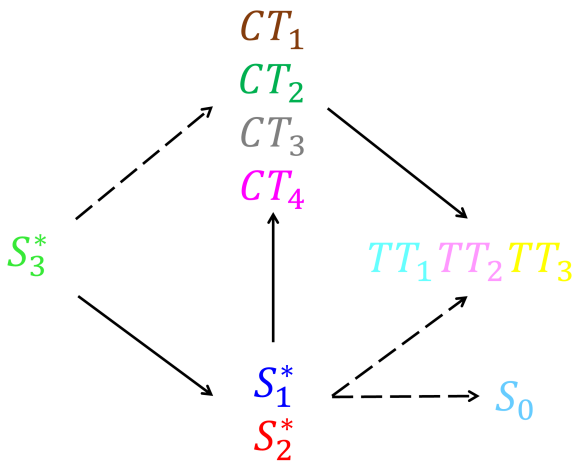

Figure 7: Schematic representation of the main net fluxes of population obtained from the nonadiabatic surface hopping simulations for the ThBF trimer using EFEM. The solid arrows indicate the main population fluxes during the dynamics, while the dashed arrows represent secondary fluxes.

The aforementioned population dynamics, obtained using EFEM, is qualitatively in good agreement with the trimer-full-QM simulations.[29] However, in the EFEM simulations, the CT states acquire a larger population compared to the trimer-full-QM, with a maximum value of $\sim$0.6 in the EFEM simulations and of $\sim$0.3 for the trimer-full-QM (see Figure 6). On the other hand, the dark excitonic states, S^*_2 and S^*_1, are less populated in the EFEM simulations with re-

spect to the trimer-full-QM, their maximum population value being ∼0.4 for EFEM (Figure 6a) and ∼0.7 for the trimer-full-QM (Figure 6b). As a consequence, in the EFEM simulations the TT states are mainly populated by transitions from the CT states and to a lesser extent by conversion from the dark excitonic states S_2^* and S_1^* (Table 3). Instead, in the trimer-full-QM most of the transitions towards the TT states take place from S_2^* and S_1^*, rather than the CT states.[29] In part, these discrepancies between EFEM and trimer-full-QM can be attributed to the fact that the starting population of CT states is larger in the EFEM simulation (0.20 versus 0.08 for trimer-full-QM). Probably more important is the larger energy decrease of the CT_1 state during the dynamics with EFEM, as it is apparent from Table 4, where we show energy differences and couplings at the transitions between pairs of excitonic states and at the beginning of the simulation. For example, CT_1 is found about 480 meV above S_1^* at $t = 0$, and drops below S_1^* (by about 40 meV) at transition times during the simulation. Although the trimer-full-QM approach shows a qualitatively similar trend (CT_1 decreases in energy by about 440 meV compared to S_1^*), the decrease in energy of the CT_1 state is quantitatively lower compared to the EFEM simulation. The faster decrease in energy of CT_1 in the EFEM simulation, if compared with trimer-full-QM, is also evident from Figure S9, where the energies of the excitonic states, averaged over all the trajectories, are reported as functions of time. According to the above discussion, the decrease in energy of CT_1 is the cause, rather than the consequence, of the increase in its population.

Additional minor differences between the EFEM and trimer-full-QM simulations can be identified in the population dynamics of the ground state (S_0) and the TT states. Specifically, in our EFEM simulations the S_0 state is populated to a slightly greater extent and the initial rise of the TT population is slightly faster, compared to the trimer-full-QM (Figure 6). At the final time of the EFEM simulations (4000 fs), the populations of the long-lived S_0 and TT states are 0.083 and 0.732 (Table S1). Assuming that the S_{1-3}^* and CT states keep decaying to S_0 and TT with the same average proportion of the first 4000 fs, we obtain the following asymptotic populations: 0.102 for S_0 and 0.898 for the TT states. Thus, in our EFEM simulations, the SF quantum yield (two triplet states for each TT state) is 1.80, which is very close to the SF yield of 1.77 extracted from the TT

asymptotic population for the trimer-full-QM.[29] This result indicates that the discrepancies in the population dynamics between EFEM and trimer-full-QM do not significantly affect the final SF quantum yield extracted from the TT states, which is almost the same in the two kinds of simulations.

Table 4: Energy differences and electronic couplings in the excitonic basis, evaluated at the starting time and at the transitions between pairs of excitonic states, averaged over the full swarm of trajectories. Energies and couplings are reported in meV.

States		at transitions			at $t = 0$	
i	j	$H_{jj} - H_{ii}$	$\lvert H_{ij}\rvert$	Time (fs)	$H_{jj} - H_{ii}$	$\lvert H_{ij}\rvert$
S_3^*	CT_1	-17	17	1171	82	9
S_3^*	CT_2	223	16	1143	259	9
S_3^*	CT_3	428	15	1221	409	8
S_3^*	CT_4	630	15	1468	570	6
S_3^*	S_2^*	-194	0	1100	-201	0
S_2^*	S_1^*	-178	0	1310	-194	0
CT_1	S_1^*	37	14	1635	-477	9
CT_1	TTS_0	-241	13	1765	-675	3
CT_1	S_0TT	-326	15	1227	-706	3
S_1^*	TTS_0	10	0	1842	-198	0
S_1^*	S_0TT	71	0	1381	-229	0

4 Conclusions

In this work, we introduced an extended Frenkel exciton model (EFEM) specifically designed for nonadiabatic dynamics simulations of multi-chromophoric systems. Our EFEM allows to describe not only the local excitations (LE) of the single chromophores (monomers) but also excited states (non-LE) belonging to chromophore pairs (dimers), such as charge-transfer and multi-excitonic states.

In our EFEM implementation, the total electronic Hamiltonian ($\mathcal{H}^{EFEM}$) is built by performing a series of QM/MM calculations, one for each selected monomer and dimer of the investigated system, in addition to a calculation at the MM level for the whole system. In our implementation, each QM/MM calculation is performed using the semiempirical FOMO-CI method. While

the energies of the LE states and the couplings between them are obtained directly from the monomeric QM/MM calculations, as in our previous work,[10] the non-LE block of $\mathcal{H}^{EFEM}$ and the couplings between LE and non-LE states are computed by constructing diabatic electronic states for each QM dimer, using a procedure based on the localization of molecular orbitals.[28] The adiabatic electronic states of the multi-chromophoric system are then computed by diagonalization of $\mathcal{H}^{EFEM}$ and the derivatives of $\mathcal{H}^{EFEM}$ with respect to the nuclear coordinates are used to determine the adiabatic energy gradients. To simulate the nonadiabatic excited state dynamics we employed Tully's fewest switches surface hopping (FSSH),[35] within its local diabatization (LD) formulation.[36] In this regard, we showed how to compute the wavefunction overlap matrix within a given time step of the dynamics using EFEM.

To validate our EFEM implementation, we investigated the singlet fission (SF) process in a trimer of ThBF molecules embedded in its crystal environment and we compared the results with those obtained in simulations based on a standard QM/MM scheme for the whole trimer (trimer-full-QM).[29] We found that EFEM satisfactorily reproduces the population dynamics for the trimer-full-QM, with moderate discrepancies mainly due to the greater involvement of the CT states in EFEM, which undergo a more pronounced energy decrease and acquire a larger population during the dynamics, compared to the trimer-full-QM. These differences in the population dynamics have little effect on the SF quantum yield extracted from the asymptotic TT population, which turned out to be essentially the same in the EFEM and trimer-full-QM simulations, indicating the suitability of our EFEM approach.

In conclusion, our implementation of EFEM combined with SH nonadiabatic dynamics enables the study of excitation energy transfer, charge transfer and multi-exciton generation in large multi-chromophoric systems. We believe that our proposed EFEM represents a promising approach for advancing our understanding of fundamental processes in complex molecular assemblies and holds promise for applications in various fields such as materials science and biological systems.

Acknowledgement

This work was supported by grants of the University of Pisa. AG and GG acknowledge funding from CN1, "HPC, Big data, Quantum Computing", Spoke 6, Multiscale Modeling and Engineering Applications.

References

(1) Turro, N. J. *Molecular Photochemistry*; W. A. Benjamin, Inc., 1967.

(2) Hernández, F. J.; Crespo-Otero, R. Modeling Excited States of Molecular Organic Aggregates for Optoelectronics. *Annual Review of Physical Chemistry* **2023**, *74*, 547–571.

(3) Mirkovic, T.; Ostroumov, E. E.; Anna, J. M.; van Grondelle, R.; Govindjee; Scholes, G. D. Light Absorption and Energy Transfer in the Antenna Complexes of Photosynthetic Organisms. *Chemical Reviews* **2017**, *117*, 249–293.

(4) Accomasso, D.; Londi, G.; Cupellini, L.; Mennucci, B. The nature of carotenoid S* state and its role in the nonphotochemical quenching of plants. *Nature Chemistry* **2024**, *15*, 2041–1723.

(5) Caffarri, S.; Broess, K.; Croce, R.; van Amerongen, H. Excitation Energy Transfer and Trapping in Higher Plant Photosystem II Complexes with Different Antenna Sizes. *Biophysical Journal* **2011**, *100*, 2094–2103.

(6) Abdullayev, N.; Kerimova, T. Influence of defects on charge and energy transfer in layered crystals. *Physica B: Condensed Matter* **2009**, *404*, 5215–5217.

(7) Sangiogo Gil, E.; Persico, M.; Granucci, G. Frenkel exciton photodynamics of self-assembled monolayers of azobiphenyls. *The Journal of Chemical Physics* **2022**, *157*.

(8) Ma, T.; Fox, E.; Qi, M.; Li, C.-H.; Sachithani, K. A. N.; Mohanty, K.; Tabor, D. P.; Pentzer, E. B.; Lutkenhaus, J. L. Charge Transfer in Spatially Defined Organic Radical Polymers. *Chemistry of Materials* **2023**, *35*, 9346–9351.

(9) Lu, Y.-C.; Diau, E. W.-G.; Rau, H. Femtosecond Fluorescence Dynamics of Rotation-Restricted Azobenzenophanes: New Evidence on the Mechanism of trans → cis Photoisomerization of Azobenzene. *The Journal of Physical Chemistry A* **2005**, *109*, 2090–2099.

(10) Sangiogo Gil, E.; Granucci, G.; Persico, M. Surface Hopping Dynamics with the Frenkel Exciton Model in a Semiempirical Framework. *Journal of Chemical Theory and Computation* **2021**, *17*, 7373–7383.

(11) Gao, F.-W.; Zhong, R.-L.; Xu, H.-L.; Su, Z.-M. Intra- and Intermolecular Charge Transfer in a Novel Dimer: Cooperatively Enhancing Second-Order Optical Nonlinearity. *The Journal of Physical Chemistry C* **2017**, *121*, 25472–25478.

(12) Ibele, L. M.; Sánchez-Murcia, P. A.; Mai, S.; Nogueira, J. J.; González, L. Excimer Intermediates en Route to Long-Lived Charge-Transfer States in Single-Stranded Adenine DNA as Revealed by Nonadiabatic Dynamics. *The Journal of Physical Chemistry Letters* **2020**, *11*, 7483–7488.

(13) Wohlgemuth, M.; Mitrić, R. Excitation energy transport in DNA modelled by multichromophoric field-induced surface hopping. *Physical Chemistry Chemical Physics* **2020**, *22*, 16536–16551.

(14) Menger, M. F. S. J.; Plasser, F.; Mennucci, B.; González, L. Surface Hopping within an Exciton Picture. An Electrostatic Embedding Scheme. *Journal of Chemical Theory and Computation* **2018**, *14*, 6139–6148.

(15) Segatta, F.; Cupellini, L.; Garavelli, M.; Mennucci, B. Quantum Chemical Modeling of the Photoinduced Activity of Multichromophoric Biosystems. *Chemical Reviews* **2019**, *119*, 9361–9380.

(16) Sisto, A.; Stross, C.; van der Kamp, M. W.; O'Connor, M.; McIntosh-Smith, S.; Johnson, G. T.; Hohenstein, E. G.; Manby, F. R.; Glowacki, D. R.; Martinez, T. J. Atomistic non-adiabatic dy-

namics of the LH2 complex with a GPU-accelerated ab initio exciton model. *Physical Chemistry Chemical Physics* **2017**, *19*, 14924–14936.

(17) Li, Z.; Hernández, F.; Salguero, C.; Lopez, S.; Crespo-Otero, R.; Li, J. Machine learning photodynamics beyond the Frenkel exciton model: Intermolecular vibrations trigger ultrafast singlet fission in pentacene crystal. *ChemRxiv* **2024**,

(18) Green, J. A.; Asha, H.; Santoro, F.; Improta, R. Excitonic Model for Strongly Coupled Multichromophoric Systems: The Electronic Circular Dichroism Spectra of Guanine Quadruplexes as Test Cases. *Journal of Chemical Theory and Computation* **2021**, *17*, 405–415.

(19) Nottoli, M.; Jurinovich, S.; Cupellini, L.; Gardiner, A. T.; Cogdell, R.; Mennucci, B. The role of charge-transfer states in the spectral tuning of antenna complexes of purple bacteria. *Journal of Chemical Theory and Computation* **2018**, *137*, 215–226.

(20) Canola, S.; Bagnara, G.; Dai, Y.; Ricci, G.; Calzolari, A.; Negri, F. Addressing the Frenkel and charge transfer character of exciton states with a model Hamiltonian based on dimer calculations: Application to large aggregates of perylene bisimide. *The Journal of Chemical Physics* **2021**, *154*, 124101.

(21) Tamura, H.; Burghardt, I.; Tsukada, M. Exciton Dissociation at Thiophene/Fullerene Interfaces: The Electronic Structures and Quantum Dynamics. *The Journal of Physical Chemistry C* **2011**, *115*, 10205–10210.

(22) Tamura, H. Diabatization for Time-Dependent Density Functional Theory: Exciton Transfers and Related Conical Intersections. *The Journal of Physical Chemistry A* **2016**, *120*, 9341–9347.

(23) Popp, W.; Polkehn, M.; Hughes, K. H.; Martinazzo, R.; Burghardt, I. Vibronic coupling models for donor-acceptor aggregates using an effective-mode scheme: Application to mixed Frenkel and charge-transfer excitons in oligothiophene aggregates. *The Journal of Chemical Physics* **2019**, *150*, 244114.

(24) Li, X.; Parrish, R. M.; Liu, F.; Kokkila Schumacher, S. I. L.; Martínez, T. J. An Ab Initio Exciton Model Including Charge-Transfer Excited States. *Journal of Chemical Theory and Computation* **2017**, *13*, 3493–3504.

(25) Cupellini, L.; Caprasecca, S.; Guido, C. A.; Müh, F.; Renger, T.; Mennucci, B. Coupling to Charge Transfer States is the Key to Modulate the Optical Bands for Efficient Light Harvesting in Purple Bacteria. *The Journal of Physical Chemistry Letters* **2018**, *9*, 6892–6899.

(26) Piteša, T.; Polonius, S.; González, L.; Mai, S. Excitonic Configuration Interaction: Going Beyond the Frenkel Exciton Model. *Journal of Chemical Theory and Computation* **2024**,

(27) Cusati, T.; Granucci, G.; Martínez-Núñez, E.; Martini, F.; Persico, M.; Vázquez, S. Semiempirical Hamiltonian for Simulation of Azobenzene Photochemistry. *The Journal of Physical Chemistry A* **2012**, *116*, 98.

(28) Accomasso, D.; Persico, M.; Granucci, G. Diabatization by Localization in the Framework of Configuration Interaction Based on Floating Occupation Molecular Orbitals (FOMO-CI). *ChemPhotoChem* **2019**, *3*, 933–944.

(29) Accomasso, D.; Granucci, G.; Wibowo, M.; Persico, M. Delocalization effects in singlet fission: Comparing models with two and three interacting molecules. *The Journal of Chemical Physics* **2020**, *152*.

(30) Persico, M.; Granucci, G. *Photochemistry: A Modern Theoretical Perspective*; Springer, Cham (Switzerland), 2018.

(31) Curutchet, C.; Mennucci, B. Quantum Chemical Studies of Light Harvesting. *Chemical Reviews* **2017**, *117*, 294–343.

(32) Madjet, M. E.; Abdurahman, A.; Renger, T. Intermolecular Coulomb Couplings from Ab Initio Electrostatic Potentials: Application to Optical Transitions of Strongly Coupled Pigments in

Photosynthetic Antennae and Reaction Centers. *The Journal of Physical Chemistry B* **2006**, *110*, 17268–17281.

(33) Persico, M.; Granucci, G. An overview of nonadiabatic dynamics simulations methods, with focus on the direct approach versus the fitting of potential energy surfaces. *Theoretical Chemistry Accounts* **2014**, *133*.

(34) Wang, L.; Trivedi, D.; Prezhdo, O. V. Global Flux Surface Hopping Approach for Mixed Quantum-Classical Dynamics. *Journal of Chemical Theory and Computation* **2014**, *10*, 3598–3605.

(35) Tully, J. C. Molecular dynamics with electronic transitions. *J. Chem. Phys.* **1990**, *93*, 1061–1071.

(36) Granucci, G.; Persico, M.; Toniolo, A. Direct semiclassical simulation of photochemical processes with semiempirical wave functions. *The Journal of Chemical Physics* **2001**, *114*, 10608–10615.

(37) Granucci, G.; Persico, M.; Accomasso, D.; Sangiogo Gil, E.; Corni, S.; Fregoni, J.; Laino, T.; Tesi, M.; Toniolo, A. MOPAC-PI: a program for excited state dynamics simulations based on nonadiabatic trajectories and semiempirical electronic structure calculations. 2024; `https://gitlab.com/granucci/mopacpi.git`.

(38) Rackers, J. A.; Wang, Z.; Lu, C.; Laury, M. L.; Lagardère, L.; Schnieders, M. J.; Piquemal, J.-P.; Ren, P.; Ponder, J. W. Tinker 8: Software Tools for Molecular Design. *Journal of Chemical Theory and Computation* **2018**, *14*, 5273–5289.

(39) Barbatti, M. et al. Newton-X Platform: New Software Developments for Surface Hopping and Nuclear Ensembles. *Journal of Chemical Theory and Computation* **2022**, *18*, 6851–6865.

(40) Stewart, J. J. P. Optimization of parameters for semiempirical methods II. Applications. *J. Comput. Chem.* **1989**, *10*, 221–264.

(41) Wibowo, M.; Persico, M.; Granucci, G. Nonadiabatic dynamics simulations of singlet fission in 2,5-bis(fluorene-9-ylidene)-2,5-dihydrothiophene crystals. *Physical Chemistry Chemical Physics* **2019**, *21*, 692–701.

(42) Persico, M.; Granucci, G.; Inglese, S.; Laino, T.; Toniolo, A. Semiclassical simulation of photochemical reactions in condensed phase. *J. Mol. Struct. THEOCHEM* **2003**, *621*, 119–126.

(43) Andersen, H. C. Molecular dynamics simulations at constant pressure and/or temperature. *The Journal of Chemical Physics* **1980**, *72*, 2384–2393.

(44) Granucci, G.; Persico, M.; Zoccante, A. Including quantum decoherence in surface hopping. *The Journal of Chemical Physics* **2010**, *133*.

(45) Persico, M.; Granucci, G.; Accomasso, D. *Reference Module in Chemistry, Molecular Sciences and Chemical Engineering*; Elsevier, 2022.

(46) Accomasso, D.; Granucci, G.; Persico, M. Singlet fission in covalent dimers of methylene-locked 1,3-diphenyl-isobenzofuran: semiclassical simulations of nonadiabatic dynamics. *J. Mater. Chem. A* **2021**, *9*, 21897–21909.

(47) Kawata, S.; Pu, Y.; Saito, A.; Kurashige, Y.; Beppu, T.; Katagiri, H.; Hada, M.; Kido, J. Singlet Fission of Non-polycyclic Aromatic Molecules in Organic Photovoltaics. *Advanced Materials* **2015**, *28*, 1585–1590.